
FOUNDATION MODEL ASSISTED WEAKLY SUPERVISED LiDAR SEMANTIC SEGMENTATION

Yilong Chen

School of Computing and Information
Chongqing University of Posts and Telecommunications
Chongqing, China
elonc@foxmail.com

Zongyi Xu

School of Computing and Information
Chongqing University of Posts and Telecommunications
Chongqing, China
xuzy@cqupt.edu.cn

Xiaoshui Huang

School of Computing and Information
Shanghai AI Laboratory
Shanghai, China
huangxiaoshui@pjlab.org.cn

Ruicheng Zhang

School of Computing and Information
CQUPT
Chongqing, China
2097170007@qq.com

Xinqi Jiang

School of Computing and Information
CQUPT
Chongqing, China
995496585@qq.com

Xinbo Gao

School of Computing and Information
Chongqing University of Posts and Telecommunications
Chongqing, China
gaoxb@cqupt.edu.com

April 22, 2024

ABSTRACT

Current point cloud semantic segmentation has achieved great advances when given sufficient labels. However, the dense annotation of LiDAR point clouds remains prohibitively expensive and time-consuming, unable to keep up with the continuously growing volume of data. In this paper, we propose annotating images with scattered points, followed by utilizing SAM (a Foundation model) to generate semantic segmentation labels for the images. Finally, by mapping the segmentation labels of the images to the LiDAR space using the intrinsic and extrinsic parameters of the camera and LiDAR, we obtain labels for point cloud semantic segmentation, and release Scatter-KITTI and Scatter-nuScenes, which are the first works to utilize image segmentation-based SAM for weakly supervised point cloud semantic segmentation. Furthermore, to mitigate the influence of erroneous pseudo labels obtained from sparse annotations on point cloud features, we propose a multi-modal weakly supervised network for LiDAR semantic segmentation, called MM-ScatterNet. This network combines features from both point cloud and image modalities, enhancing the representation learning of point clouds by introducing consistency constraints between multi-modal features and point cloud features. *On the SemanticKITTI dataset, we achieve 66% of fully supervised performance using only 0.02% of annotated data, and on the NuScenes dataset, we achieve 95% of fully supervised performance using only 0.1% labeled points.*

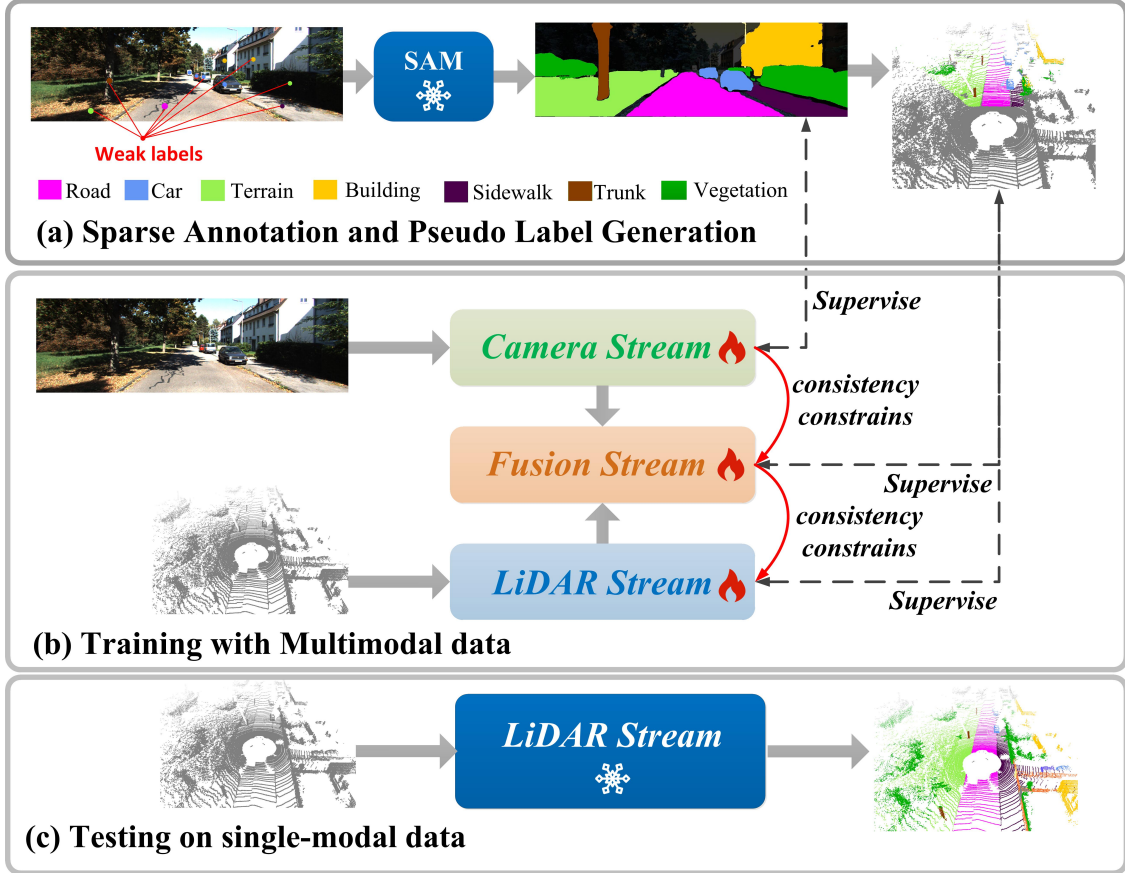


Figure 1: Our Multimodal Weakly Supervised LiDAR Segmentation Pipeline. (a) Sparse Annotation and Pseudo-Label Generation: Sparse labels on images are used to generate dense pseudo-labels for point cloud, requiring minimal annotation effort. (b) Training with Multimodal Data: Incorporating image features enhances point cloud representations, mitigating errors in pseudo-labels during training. (c) Testing on Single-Modal Data: Predictions are made solely using LiDAR input, simplifying deployment without image inputs.

1 Introduction

In recent years, weakly supervised point cloud semantic segmentation has attracted widespread research attention that only uses fewer annotations to achieve comparable performance with the fully-supervised counterparts [1, 2]. These methods can be categorized based on how point clouds are obtained, namely RGB-D scanning-based and LiDAR scanning-based approaches. Among these, scenarios based on LiDAR scanning are the most challenging, as LiDAR point clouds have a broader scale range and uneven density distribution compared to RGB-D point clouds. Therefore, it is difficult to achieve competitive performance with fully supervised methods when only a small number of labeled points are available, which is also the primary focus of our paper. Existing research has mostly focused on designing network architectures and loss functions to fully utilize limited sparse annotations, but there is little research attention on how to expand limited sparse labels. Some studies attempt to predict pseudo-labels using existing sparse labels [3, 4]; however, due to model constraints, this approach results in low-quality pseudo-labels. To address the aforementioned challenges, we for the first time employ SAM [5] (a foundation model for image segmentation) to expand the original sparse annotations. The specific method can be divided into three processes, as shown in Figure 1.

(a) Sparse Annotation and Pseudo-Label Generation. In typical point cloud scenarios, such as autonomous driving, there often involve camera sensors alongside auxiliary LiDAR sensors. By synchronizing and calibrating the LiDAR and camera sensors, a clear mapping between 3D and 2D data in terms of point-to-pixel transformation is established. Leveraging this intrinsic physical spatial relationship, we first construct a weakly supervised LiDAR semantic segmentation dataset using scattered annotations on images. Specifically, we annotate sparse labels only on images, where the number of annotations for each class is based on the proportion of pixels occupied by that class in the image. Subsequently, a pre-trained foundation model, specifically SAM [5], is employed to obtain semantic

segmentation results from the sparse annotations on images. Finally, semantic labels from images are mapped into the LiDAR coordinate system, thereby generating dense 3D pseudo-labels from sparse annotations, as illustrated in Figure 1(a). Unlike [6, 7] that require obtaining full segmentation labels for images beforehand, our method only requires 1-5 annotation labels per class, thus saving time and effort associated with intensive annotation tasks.

(2) Training with Multimodal data. While SAM [5] can convert sparse labels into dense semantic labels, these pseudo-labels often contain numerous errors. To mitigate the impact of erroneous pseudo-labels on performance during training, we use image features to enhance point cloud representations and train the network through multi-modal consistency constraints to reduce the adverse effects of erroneous pseudo-labels on model training, as shown in Figure 1(b). Unlike [8, 9] that directly concatenate two modal features for fusion, we introduce a fusion network between the point cloud and image modalities to reduce the gap between modalities and enhance point cloud features through perceptual consistency constraint losses.

(c) Testing on single-modal data. During the testing phase, we predict solely using the LiDAR modality as input. This allows deployment without the need for image inputs.

Our experiments demonstrate that the proposed framework achieves **over 66% of fully supervised learning performance on SemanticKITTI using only 0.02% of annotated data and over 75% on NuScenes using only 0.1% of annotated data**. Further extensive ablation studies confirm the effectiveness of the modules proposed in our framework.

The contributions in this work are summarized follows:

- We introduce Scatter-KITTI and Scatter-NuScenes, two datasets for LiDAR semantic segmentation utilizing scattered annotations on images.
- We propose MM-ScatterNet, which designs a fusion branch to integrate image and point cloud features and ultimately obtain enhanced point cloud features through perceptual consistency constraint losses.
- Based on the scattered annotation process, we achieved performance levels of up to 66% relative to fully supervised training using only 0.02% labeled points on SemanticKITTI [10] and over 75% on NuScenes [11] using only 0.1% labeled points.

2 Related Work

2.1 Fully-supervised Point Cloud Segmentation

Existing point cloud semantic segmentation methods based on single-modal can be divided into four categories: **point-based, projected-based, voxel-based and multi-representation fusion**. The **point-based** method directly takes the original point cloud as input and outputs each point label. PointNet [12] was the pioneer of this type of method, and there have been many improvements based on it [13, 14, 15, 16, 17, 18, 19, 20, 21, 22]. The advantage of point based methods is that they are data-driven. However, since the need for local sampling of points in this method, the memory requirement increases sharply with the increase in the number of points. Therefore, this type of method is currently mainly used in indoor scenes with fewer point clouds, rather than outdoor scenes. The **projected-based** method does not require significant memory overhead. This method projects the 3D LiDAR onto the 2D coordinate system based on the internal and external parameter matrices of the camera and LiDAR, allowing for direct utilization of algorithm models from image segmentation, such as FCN [23] and UNet [24]. According to different projection strategies, projected-based method can be divided into: Mulit-view segmentation [25, 26, 27], Range Image or BEV (Bird eye view) segmentation [28, 29, 30, 31], and multi view fusion methods [32, 33]. As converting 3D LiDAR into 2D images for processing, the original spatial structure information of 3D data is lost. Most recent works have adopted **voxel-based** as they balance efficiency and effectiveness, with SparseConv [34] being the most commonly used. Unlike traditional voxel methods that directly convert point clouds into voxels, sparse convolution only stores non empty voxels in a hash table and only performs convolution on non empty voxels, resulting in high computational efficiency. Currently, many studies have adopted SparseConv to design more powerful network architectures [35, 36]. Very recently, there is a trend of exploiting **Multi-Representation Fusion** methods. These methods combine multiple representations above (i.e., points, projection images, and voxels) and design feature fusion among different branches [37, 38]. However, these methods only use sparse and textureless LiDAR point clouds as input, so texture information in camera images is not fully utilized.

2.2 Multimodal point cloud segmentation

Multimodal methods attempt to fuse information from two complementary sensors and utilize the benefits of both camera and LiDAR. However, because 3D point clouds and 2D images are in different metric space, it is difficult to fuse

them directly by convolution stitching or attention mechanism. To solve this problem, one solution is to use a 3D object detection method to project a 3D point cloud into 2D space [39, 40], so that the point cloud and image are in the same coordinate system [41]. The advantage of this type of method is that it can directly utilize existing two-dimensional image segmentation methods to process the projected point cloud. In addition, since the projected point cloud is in the same coordinate system as the image, it can effectively fuse the intermediate feature layers. However, this method requires both image and point cloud data to be input during the inference stage, so in practical applications, multimodal features need to be aligned on timestamps. To address the aforementioned difficulties, another solution is to lift 2D image features into 3D space. xMUDA [42] used a 2D image segmentation network and a 3D sparse convolutional network [37] to process 2D images and 3D point cloud data, respectively. Since there is no fusion of intermediate layer features, the image processing network can be completely discarded during testing. However, it is difficult for the network to fully utilize appearance and texture in the camera images. In order to facilitate the fusion of intermediate layer features, Xu Yan et al. [43] recently proposed a network called 2DPASS, which concatenates the features of images and point clouds during the feature decoding stage. However, the above methods only use information shared by the two modalities when fusing multimodal features, while ignoring the unique private information of image modalities. In addition, when using distillation knowledge for information extraction, there is no reasonable perception of the difference between multimodal and single modal features, resulting in the extraction of fusion information with low confidence into the target modality when multimodal features are weaker than single modal features.

2.3 Weakly-supervised Point Cloud Segmentation

In order to reduce annotation costs, some recent work has delved deeply into the field of Weakly Supervised Semantic Segmentation (WSSS) methods [44]. These methods can be categorized based on different levels of supervision, including partially labeled points [45, 2, 46], sub-cloud level annotations [47], and scene-level annotations [47, 48]. Among several weak labeling schemes, the partially point labeling scheme provides the best balance between annotation cost and segmentation performance [49, 50], which is also the focus of our paper. Existing methods employ various techniques to enhance the performance of models, which can roughly be divided into two categories: pseudo-labeling and consistency regularization. Pseudo-labeling methods predict pseudo-labels for unlabeled points to explore them. MPRM [47] trains segmentation models on sub-cloud labels and uses class activation mapping [51] to pseudo-label entire sub-clouds for training the final model. OTOC [45] improves the quality of pseudo-labels through multiple rounds of self-training. SQN [49] better utilizes limited labels by leveraging geometric priors. However, utilizing pseudo-labels for model iteration optimization often suffers from the influence of unreliable pseudo-labels, resulting in poor segmentation performance. Therefore, consistency regularization reduces the impact of unreliable labels in weakly supervised point cloud semantic segmentation by imposing consistency constraints on the predicted distributions after the model function. [52]utilizing a sufficient smoothness constraint by applying a large amount of unlabeled 3D points for weakly supervised point cloud segmentation. [48, 53] Fully exploiting the point feature affinities from multiple data modalities for the constraint of multimodal features. [54] A novel Hybrid Contrastive Regularization (HybridCR) framework, employed in weakly supervised settings, exhibits competitiveness in performance compared to its fully supervised counterparts. Our approach combines the advantages of the above two categories of methods. For generating pseudo-labels, we diverge from previous methods that directly generate pseudo-labels from point clouds. Instead, we first expand 2D sparse labels into dense pseudo-labels using SAM [5]. Then, based on the mapping relationship between images and point clouds, we map the dense 2D pseudo-labels to corresponding 3D point labels, thus achieving the goal of pseudo-label generation.

Regarding consistency regularization, we fuse point cloud and image modalities. By constraining the prediction results of the point cloud modality to be consistent with the prediction results of the fused modality, we provide additional consistency supervision for point cloud features, ultimately enhancing point cloud features. It’s important to note that while obtaining 3D pseudo-labels, we also generate 2D per-pixel pseudo-labels. This allows us to provide pixel-level supervision for image features, which differs from the sparse supervision at the point level as in [53]. As a result, we obtain more accurate image features, enabling more precise multi-modal fusion features.

3 The Scatter-KITTI and Scatter-NuScenes dataset

Although LiDAR point cloud semantic segmentation has become increasingly popular in recent years, the quantity of large-scale datasets remains limited due to the complexity and time-consuming nature of the data annotation process. We propose to tackle this issue by utilizing sparse annotations from 2D images for LiDAR segmentation, and we introduce Scatter-KITTI and Scatter-NuScenes, the first LiDAR point cloud datasets annotated with sparse annotations. We choose SemanticKITTI [10] and NuScenes [11] because they are currently widely used and have established benchmarks.

3.1 Data Annotation

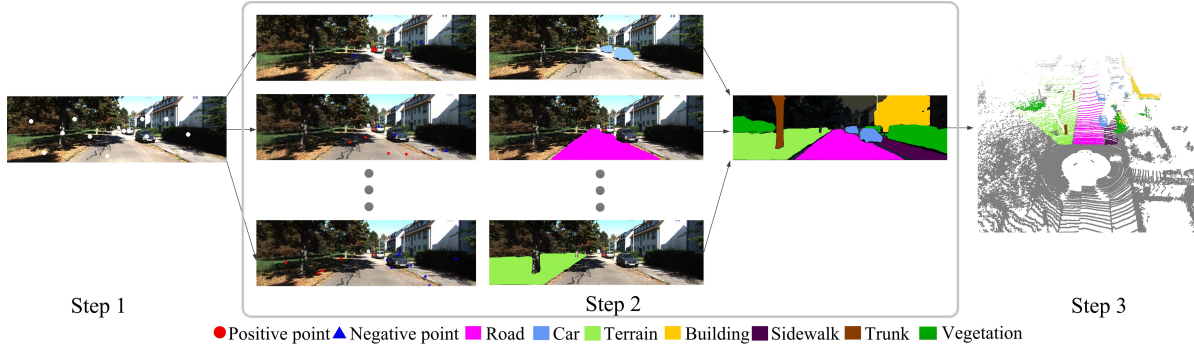


Figure 2: Scatter annotation process: Step 1: Generating 2D sparse labels by projecting point cloud labels onto images and randomly selecting 1-5 labels per class. Step 2: Predicting 2D dense labels using SAM [5] to generate segmentation masks for each class. Step 3: Obtaining 3D pseudo-labels by mapping predicted dense labels back to 3D space.

The annotation process can be divided into three steps, as shown in Figure 2. **Step 1:** Generating 2D sparse labels. We project the point cloud labels onto images using the intrinsic and extrinsic matrices of the camera and LiDAR. Then, we randomly select points and retain 1-5 labels for each class based on the size of the image pixel area occupied by each class. Since our labels are randomly determined, we can avoid biases introduced by manual annotation.

Step 2: Predicting 2D dense labels. Utilizing SAM [5], a semantic segmentation large model, we first generate segmentation masks for each class. For example, to generate a mask for cars, we consider point labels of cars as positive sample points, while point labels of other classes (such as trees, grass, buildings, etc.) are considered negative sample points. Then, we feed the positive and negative point labels along with the image into the pre-trained SAM [5] model to obtain the segmentation mask for that class. Subsequently, we generate segmentation masks for each class sequentially and merge all the segmentation masks to obtain the final segmentation result.

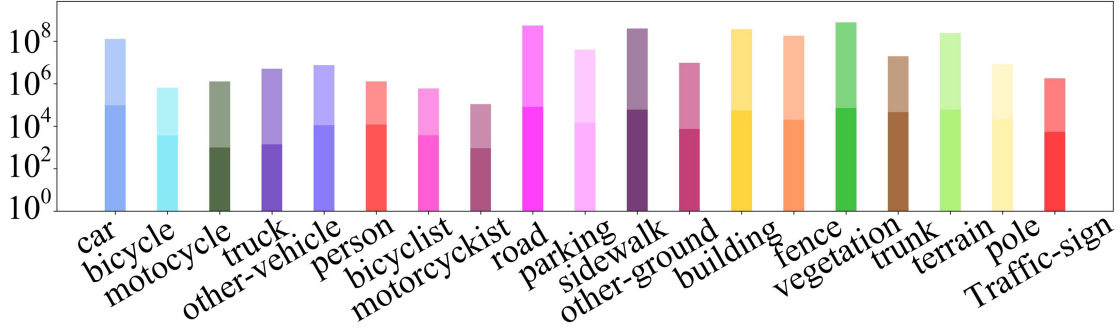
Step 3: Obtaining 3D pseudo-labels. Building upon the step 2, we utilize the intrinsic relationship between the camera and LiDAR in physical space to map the predicted dense labels back to 3D space, thus obtaining labels for points. Using the aforementioned method, we generate pseudo-labels for both the SemanticKITTI and NuScenes datasets, and refer to the sparse labels obtained from the step 1 as Scatter-KITTI and Scatter-NuScenes, respectively. Further information about the annotation process is provided in the supplementary materials.

3.2 Statistics and visualization results

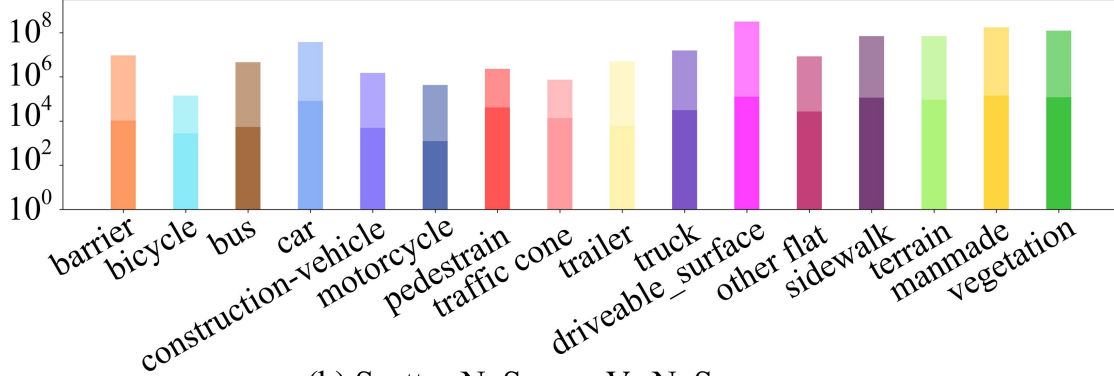
We annotated the training sets of SemanticKITTI [10] based on KITTI [55], which employs a 64-line LiDAR and comprises 11 sequences, 23,200 scans, and 2.848 billion points. Scatter-KITTI contains 0.55 million labeled points, equivalent to only 0.02% of the total points. We retained the same 19 categories to facilitate a smooth transition to scatter-supervised LiDAR semantic segmentation research. The distribution of category labels can be seen in Figure 3(a).

We also conducted sparse annotations on the training set of NuScenes [11], which uses a 32-line LiDAR and includes 10 scenes, 34,149 scans, and 1.185 billion points. Scatter-NuScenes contains 1.08 million labeled points, equivalent to only 0.1% of the total points. We retained the same 17 categories to encourage a smooth transition to scatter-supervised LiDAR semantic segmentation research. The distribution of category labels can be seen in Figure 3(b).

Pseudo-label Accuracy Analysis: We computed the accuracy of 3D pseudo-labels generated from Scatter-KITTI and Scatter-NuScenes, yielding average accuracies of 85% and 89%, respectively. Additionally, we conducted a per-category analysis of the accuracy of generated 3D pseudo-labels, as depicted in Figure 4. From Figure 4, it can be observed that while the overall label accuracy is high, accuracy for small objects is less than 50%. To mitigate the uncertainty introduced by erroneous pseudo-labels, we propose our MM-ScatterNet in Section.4.2, which reduces this effect through multimodal consistency constraints. Visualizations of point cloud pseudo-labels obtained from Scatter-KITTI and Scatter-NuScenes are presented in Figures 5 and 6, respectively. Due to differences in field of view (FOV) between cameras and LiDAR, point cloud pseudo-labels obtained from Scatter-KITTI cover only partial regions, whereas those from Scatter-NuScenes cover 360°.



(a) Scatter-KITTI VS SemanticKITTI



(b) Scatter-NuScenes Vs NuScenes

Figure 3: Number of Labeled Points Comparison. Light colors represent SemanticKITTI and NuScenes, while dark colors represent Scatter-KITTI and Scatter-NuScenes. (a) Number of points labeled in Scribble-KITTI visualized against SemanticKITTI in log-scale; (b) Number of points labeled in Scribble-NuScenes visualized against NuScenes in log-scale.

4 Scatter-Supervised LiDAR Segmentation

We elaborately designed a multimodal fusion framework for handling scatter-supervised LiDAR segmentation, which is called MM-ScatterNet. By integrating image features and proposing a perceptual consistency loss, we enhance the representation learning of point clouds. Figure 7 illustrates the overall architecture, which can be divided into the following three parts: (1) point-to-pixel correspondence, (2) multimodal fusion framework, and (3) perceptual consistency loss.

4.1 Point to pixel Correspond

Considering the fact that 2D features and 3D features are typically represented as pixels and points, it is difficult to directly transfer information between the two modalities. In order to fuse the features of images and point clouds, we conducted two stages of fusion through the mapping relationship between point clouds and pixels. In the first stage, we follow [41] and adopt perspective projection to project a 3D point cloud onto a 2D image coordinate system. Specifically, Let $\mathbf{P} = \{p_i\}_{i=1}^N \in \mathbb{R}^{N \times 3}$, be the projection of each 3D point $p_i = (x_i, y_i, z_i) \in \mathbb{R}^3$ to a point $\hat{p}_i = (u_i, v_i) \in \mathbb{R}^2$ in the image plane is given as:

$$[u_i, v_i, 1]^T = \frac{1}{z_i} \mathbf{T} \times \mathbf{R} \times [x_i, y_i, z_i, 1]^T. \quad (1)$$

Where $\mathbf{T} \in \mathbb{R}^{3 \times 4}$ and $\mathbf{R} \in \mathbb{R}^{4 \times 4}$ are the camera intrinsic and extrinsic matrices respectively provided in Dataset.

Let $\mathbf{X}_{img} \in \mathbb{R}^{3 \times H \times W}$ be an image from an RGB camera, where H and W indicate the height and width of image, respectively. Let $\mathbf{X}_{point} \in \mathbb{R}^{N \times C}$ be point clouds from LiDAR, where N and C indicate the number of point and the

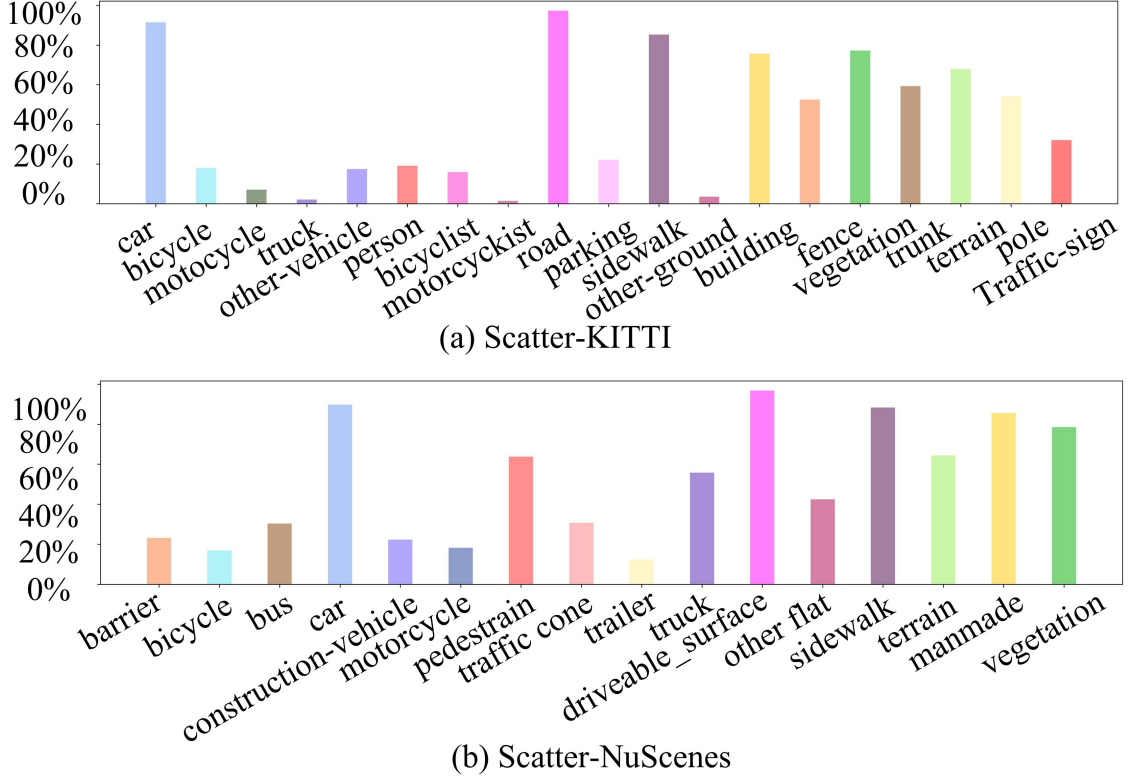


Figure 4: Pseudo-label Accuracy for Each Class

3D LiDAR features. Let $\mathbf{X}_{proj} \in \mathbb{R}^{C \times H \times W}$ be the 2D LiDAR features that projects the point clouds onto a 2D image coordinate system according to the Eq.(1).

Since the sparsity of the point cloud, each pixel in the projected \mathbf{X}_{proj} may not have a corresponding point \mathbf{P} . Therefore, we first initialize all pixels in to 0. Following [41], we then compute 5-channel LiDAR features, i.e., (d, x, y, z, i) , for each pixel (h, w) in the \mathbf{X}_{proj} , where $d = \sqrt{x^2 + y^2 + z^2}$. and i represents the intensity of point cloud. The specific fusion details will be described in Section 4.2.

After the projection, the point-to-pixel mapping is represented as:

$$M_{p \rightarrow i} = \{[v_i], [u_i]\}_{i=1}^N \in \mathbb{R}^{N \times 2} \quad (2)$$

Where $[\cdot]$ is the floor operation.

In the second stage, following Eq.(2), we utilize the mapping relationship between points and pixels, to lift the 2D features fused in the first stage to 3D space, thereby facilitating fusion with 3D point cloud features. The detailed fusion process will be introduced in section 4.2.

4.2 Architecture of MM-ScatterNet

Since image and point cloud modal data are in different metric space, it is difficult to use a single network to process two types of data from different modes. Motivated by [43], We propose a multi branch network structure consisting of three parts: **Camera Stream**, **Fusion Stream**, and **LiDAR Stream**, which are respectively used to extract image features, point cloud features, and fuse these two modal features, as illustrated in Figure 7. To the end, We effectively fuse point cloud and image information by designing a separate 2D modal fusion network.

Let M_{point} , M_{img} , and M_{fuse} be the camera, LiDAR and fusion stream in MM-ScatterNet, respectively. Let $O^{point} \in \mathbb{R}^{N \times S}$, $O^{img} \in \mathbb{R}^{S \times H \times W}$ and $O^{fuse} \in \mathbb{R}^{S \times H \times W}$ be output probabilities with respect to each network, where S indicate the number of semantic classes. Please note that each branch has 4 scales of output and classification

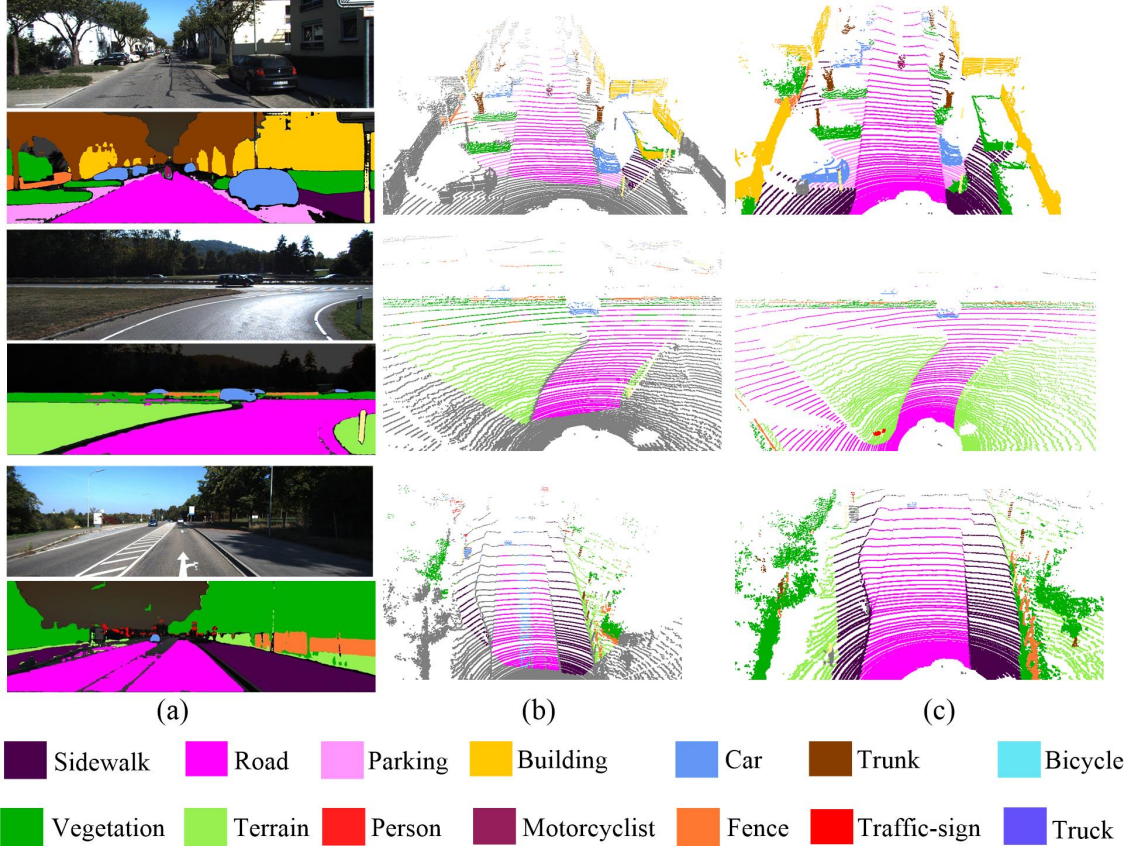


Figure 5: Visualizing the results of Step 2 and Step 3 in the Scatter annotation process on the Scatter-KITTI dataset. (a) 2D dense labels obtained in Step 2, (b) 3D pseudo-labels obtained in Step 3. (c) Ground Truth Labels

heads. To simplify the description, we use one of these scales as an example. The outputs of MM-ScatterNet are computed by

$$\begin{cases} O^{img} = M_{img}(X_{img}), \\ O^{point} = M_{point}(X_{point}), \\ O^{fuse} = M_{fuse}(X_{proj}). \end{cases} \quad (3)$$

For the **Camera stream**, Following [43] we crop the image into smaller patches as input data for the network. We apply ResNet34 [56] encoder with 2D convolution as 2D network and adopt UNet [24] decoder to up-sample the features from each encoder layer. For the **LiDAR stream**, we adopt sparse convolution to encode the feature from point cloud. For the up-sampling part, we adopt the approach proposed in [43]. Please refer to the paper for future details.

For the **Fusion stream**, we fuse the image and point cloud through two stages. In the first stage, we fuse the features of the image from Camera stream with the point cloud projected into 2D image plane. Let $\{\mathbf{F}_l^{img} \in \mathbb{R}^{C_l^{img} \times H_l \times W_l}\}_{l=L}^L$ represent a set of image features from the camera stream, where l indicates the layer in which we obtain the features, C_l indicates the number of channels of the l -th layer in the camera stream, and H_l and W_l indicate the height and width of the feature maps from the l -th layer, respectively. Let $\{\mathbf{F}_l^{proj} \in \mathbb{R}^{C_l^{proj} \times H_l \times W_l}\}_{l=L}^L$ stand for the Fusion stream that only contains point cloud features projected onto the image coordinate system, where C_l^{proj} indicates the number of channels of the l -th layer in the Fusion stream. We first concatenate the features of \mathbf{F}_l^{img} and \mathbf{F}_l^{proj} and use a convolutional layer to reduce the number of channels of the fused features that are shown in Eq.(4).

$$\mathbf{F}_l^{fuse_2D} = f_l([\mathbf{F}_l^{img}; \mathbf{F}_l^{proj}]). \quad (4)$$

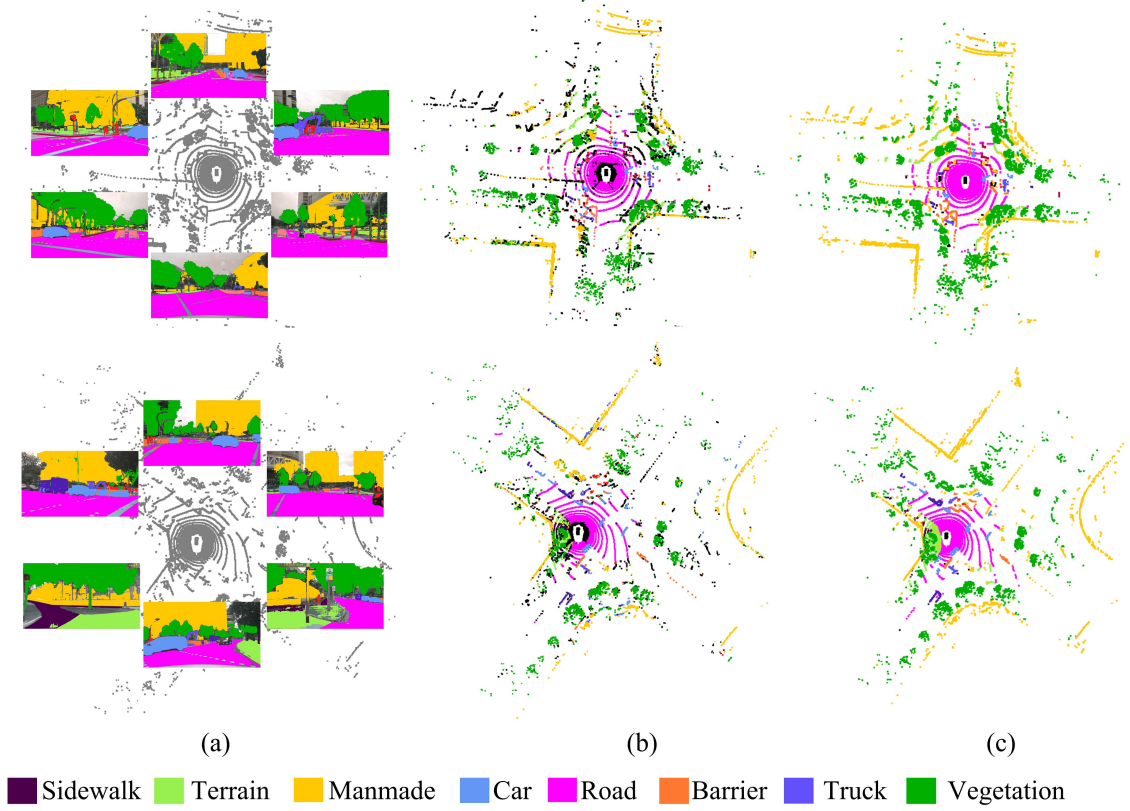


Figure 6: Visualizing the results of Step 2 and Step 3 in the Scatter annotation process on the Scatter-NuScenes dataset. (a) 2D dense labels obtained in Step 2, (b) 3D pseudo-labels obtained in Step 3. (c) Ground Truth Labels

Where $[\cdot; \cdot]$ indicates the concatenation operation. $f_l(\cdot)$ is the convolution operation w.r.t. the l -th the fusion module.

And then, we used residual modules and attention modules (see Figure 7(a)) to obtain the fusion features of the first stage by

$$\mathbf{F}_l^{fuse_2D} = \mathbf{F}_l^{img} + \sigma(g_l(F_l^{fuse_2D})) \odot F_l^{fuse_first} \quad (5)$$

In the second stage, Let $\{\mathbf{F}_l^{point} \in \mathbb{R}_l^{N \times C_l^{point}}\}_{l=1}^L$ be the features from LiDAR stream, where C_l^{point} indicates the number of channels of l -th layer in LiDAR stream, N indicates the number of point clouds. In order to fuse point cloud features \mathbf{F}_l^{point} into the Fusion Stream, we first lift the fused features in the first stage $\mathbf{F}_l^{fuse_2D}$ to 3D space based on the mapping relationship between point clouds and pixels in Eq.(2).

And then, using the same fusion method as in the first stage, to fuse \mathbf{F}_l^{point} and $\mathbf{F}_l^{fuse_2D}$. The final fused features $\mathbf{F}_l^{fuse_3D}$ are calculated as follows:

$$\begin{cases} \mathbf{F}_l^{fuse_3D} = f_{MHA}([\mathbf{F}_l^{fuse_2D}; \mathbf{F}_l^{point}]) + \mathbf{F}_l^{point} \\ \mathbf{F}_l^{fuse_3D} = \mathbf{F}_l^{3D} + MLP(\mathbf{F}_l^{fuse_3D}) \end{cases} \quad (6)$$

In which MHA represents Multi-Head Attention, and MLP represents Multi-Layer Perceptron, as illustrated in Figure 7(c).

4.3 Construction of Perceptual consistency loss

The construction of Perceptual consistency loss is significant in our MM-ScatterNet. As demonstrated in Figure1, in order to determine which information needs to be fused and which needs to be discarded during the fusion process, inspired by [41], we extract strong confidence features from the fusion mode and image mode into the point cloud mode by perceiving the differences between different modes. Different from [41], Our perceptual consistency loss

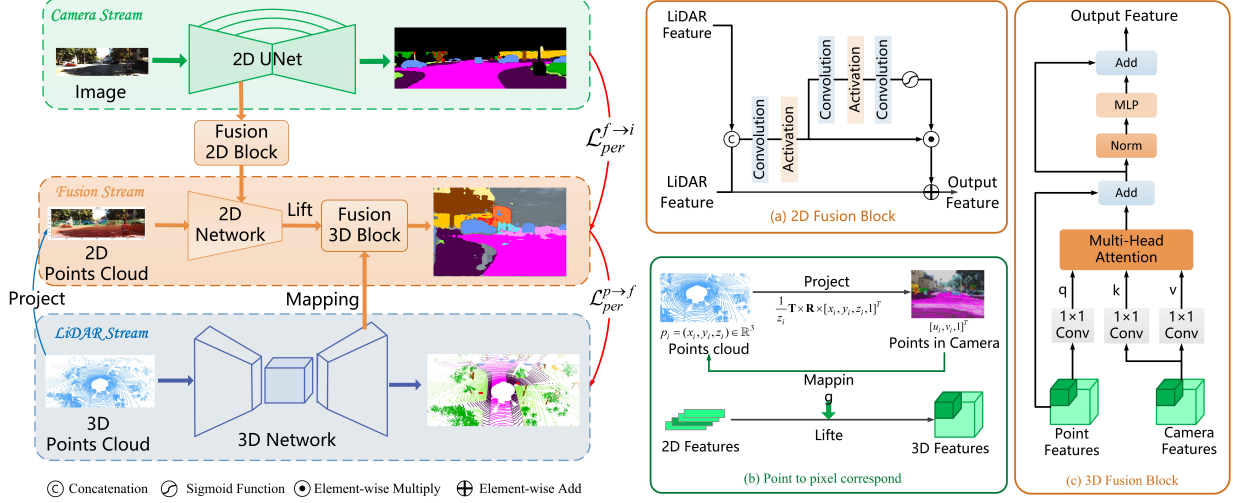


Figure 7: Overview of the proposed MM-ScatterNet. Input: We crops small patch from the original camera image as the Camera stream input. Then, the LiDAR projected onto the image plane and itself will independently pass through the Fusion and LiDAR stream. Fusion: the image features will be fused with the point cloud projected onto image plane and then the fused 2D features are lifted to 3D space based on pixel-to-point correspond. Finally, the 3D point clouds could be fused with 2D features to obtain the final fused features. Consistency Constraint: By using KL divergence, the image features, fusion features, and point cloud features are made consistent.

consists of two parts: consistency between image and fusion features, and consistency between point cloud and fusion features. Detailed discussion will be carried out in the Section 5.2.3.

To measure the perceptual confidence of the predictions with respect to the Camera stream, LiDAR stream and Fusion stream, we first compute the three entropy maps $\mathbf{E}_i^{img} \in \mathbb{R}^{H \times W}$, $\mathbf{E}_i^{point} \in \mathbb{R}^{H \times W}$ and $\mathbf{E}_i^{fuse} \in \mathbb{R}^{H \times W}$ respectively by

$$\begin{cases} \mathbf{E}_i^{img} = -\frac{1}{\log^S} \sum_{s=1}^S \mathbf{O}_{i,s}^{img} \log(\mathbf{O}_{i,s}^{img}) \\ \mathbf{E}_i^{point} = -\frac{1}{\log^S} \sum_{s=1}^S \mathbf{O}_{i,s}^{point} \log(\mathbf{O}_{i,s}^{point}) \\ \mathbf{E}_i^{fuse} = -\frac{1}{\log^S} \sum_{s=1}^S \mathbf{O}_{i,s}^{fuse} \log(\mathbf{O}_{i,s}^{fuse}) \end{cases} \quad (7)$$

Following [57], we use \log^S to normalize the entropy to (0,1]. The perceptual confidence map \mathbf{C}_{img} , \mathbf{C}_{point} and \mathbf{C}_{fuse} with respect to the Image stream, LiDAR stream and Fusion stream are computed by $\mathbf{C}_{img} = 1 - \mathbf{E}_{img}$, $\mathbf{C}_{point} = 1 - \mathbf{E}_{point}$ and $\mathbf{C}_{fuse} = 1 - \mathbf{E}_{fuse}$. Note that not all information from the Image stream and Fusion stream are useful. Inspired by [41, 42], the predictions with lower confidences scores are more likely to be wrong. Combining confidence thresholds, we measure the importance of perceptual information from Image stream and LiDAR stream by

$$\begin{cases} \Omega_i^{f \rightarrow p} = \begin{cases} \max(\mathbf{C}_{fuse} - \mathbf{C}_{point}), & \text{if } \mathbf{C}_{fuse} > \tau \\ 0, & \text{otherwise.} \end{cases} \\ \Omega_i^{i \rightarrow p} = \begin{cases} \max(\mathbf{C}_{img} - \mathbf{C}_{fuse}), & \text{if } \mathbf{C}_{img} > \tau \\ 0, & \text{otherwise.} \end{cases} \end{cases} \quad (8)$$

Here τ indicates the confidence threshold.

Finally, we can build Our perceptual consistency loss to extract information from a single mode (camera stream) and a multi-mode (Fusion stream) to the target mode (LiDAR stream), as shown in Eq.(9):

$$\begin{cases} \mathcal{L}_{per}^{f \rightarrow i} = \frac{1}{N} \sum_{i=1}^N \Omega_i^{f \rightarrow i} D_{KL}(\mathbf{O}^{fusion} || \mathbf{O}^{img}) \\ \mathcal{L}_{per}^{p \rightarrow f} = \frac{1}{N} \sum_{i=1}^N \Omega_i^{p \rightarrow f} D_{KL}(\mathbf{O}^{point} || \mathbf{O}^{fuse}) \end{cases} \quad (9)$$

Where N is the number of point cloud projected onto the image plane and $D_{KL}(\cdot || \cdot)$ indicates the Kullback-Leibler divergence [58].

Apart from the uni-directional perception-aware loss, we also use Cross entropy loss and Lov'asz-softmax loss [59], which are commonly used in existing semantic segmentation task, to train the network. The objective w.r.t. the Camera, LiDAR and Fusion stream are defined by

$$\begin{cases} \mathcal{L}_{Camera} = \mathcal{L}_{ce} + \mathcal{L}_{lov} + \lambda \mathcal{L}_{per}^{f \rightarrow i} \\ \mathcal{L}_{Fusion} = \mathcal{L}_{ce} + \mathcal{L}_{lov} + \gamma \mathcal{L}_{per}^{p \rightarrow f} \\ \mathcal{L}_{Point} = \mathcal{L}_{ce} + \mathcal{L}_{lov} \end{cases} \quad (10)$$

5 Experiments

We conducted experiments using state-of-the-art point cloud semantic segmentation models in recent years, but omitted the application of Test-Time Augmentation (TTA) during testing, and evaluated performance on fully annotated SemanticKITTI [10] and NuScenes [11] validation sets unless otherwise stated. In addition to mean Intersection over Union (mIoU), we also provide the relative performance between Scatter Supervision Training (SS) and Fully Supervised Upper Bound (FS), expressed as a percentage (SS/FS).

Implementation Details: We set the learning rate starts at 0.24 and decays to 0 with a cosine annealing algorithm. The batch size to 8 on Scatter-KITTI and 4 on Scatter-nuScenes. We set λ, γ to 0.2, 0.5, respectively. In addition, we also used a series of data augmentation to prevent overfitting in the training step, including random cropping, instance augmentation, random horizontal flipping, color jitter.

5.1 Results

In Table 1 and Table 2, we present the LiDAR segmentation results from the SemanticKITTI [10] and NuScenes [11] validation sets, respectively, using three state-of-the-art networks (MinkowskiNet [60], SPVCNN [37], and Spherical transformer [61]) to demonstrate the model-independence of our approach. In Figure 8, we show case the visual results on the SemanticKITTI [10] validation set using SPVCNN [37].

From Table 1 and Table 2, it can be observed that the performance decreases compared to fully supervised methods due to the lack of available supervision. Specifically, the relative performance (SS/FS) of the models on the Scatter-KITTI dataset is 64.0%, 64.7%, and 67.1% relative to their respective fully supervised upper bounds. By employing our proposed MM-ScatterNet, we are able to significantly narrow the gap between the two training strategies, resulting in relative performances of 67.4%, 68.4%, and 68.9% for all three models, respectively.

Scatter as Annotation: We compared our annotation strategy with other labeling strategies in Table 3 and Table 4. While our method is weaker in terms of relative performance compared to existing methods, we want to emphasize that our labeling strategy can reduce 75% of the labeled points compared to the state-of-the-art methods. This means we can spend less time annotating point clouds.

5.2 Ablation study

To demonstrate the contributions of different components in our MM-ScatterNet, we conducted ablation experiments on the Scatter-KITTI dataset, and for fair comparison, the point cloud processing network was uniformly adopted as SPVCNN [60].

5.2.1 Effect of Network components.

The results of the ablation experiment are shown in Table 5. Our baseline model achieved a lower result of 40.6% on mIoU as a result of only using point cloud mode. When image information is added to the fusion module, the segmentation effect can be significantly improved, with a mIoU of 41.8%. This improvement mainly benefits from the

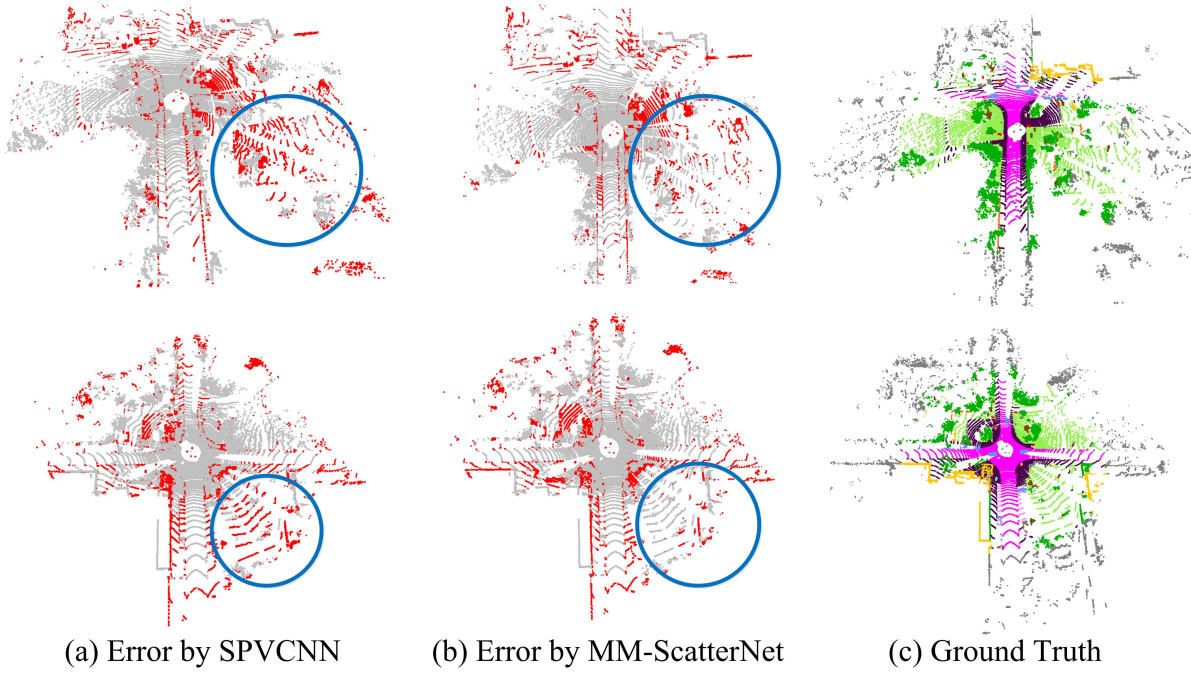


Figure 8: Example results from the SemanticKITTI valid-set comparing (c) the ground truth frame; to SPVCNN [37] trained (a) scatter-supervised, and (b) scatter-supervised using our MM-ScatterNet.

Table 1: LiDARsegmentation results evaluated on the SemanticKITTI valid-set.

Model	Supervision	our	mIoU(%)	SS/FS(%)
MinkowskiNet [60]	Fully		61.4	-
	Scatter-KITTI		39.3	64.0
	Scatter-KITTI	✓	41.4	67.4
SPVCNN [37]	Fully		63.6	-
	Scatter-KITTI		40.6	64.7
	Scatter-KITTI	✓	43.8	68.8
Spherical [61]	fully		64.8	-
	Scatter-KITTI		43.5	67.1
	Scatter-KITTI	✓	44.7	68.9

Table 2: LiDAR segmentation results evaluated on the Nuscenes valid-set.

Model	Supervision	our	mIoU(%)	SS/FF(%)
MinkowskiNet [60]	Fully		66.4	-
	Scatter-Nuscenes		48.2	72.5
	Scatter-Nuscenes	✓	50.1	75.4
SPVCNN [37]	Fully		68.5	-
	Scatter-Nuscenes		49.3	71.9
	Scatter-Nuscenes	✓	51.6	75.3
Spherical [61]	fully		70.3	-
	Scatter-Nuscenes		50.9	72.4
	Scatter-Nuscenes	✓	52.8	75.1

Table 3: Quantitative results of the various approaches on SemanticKITTI validation set

Method	Annot.	mIoU(%)	SS/FS(%)
Scribble [62]	8%	61.9	96.3
ReDAL [63]	5%	59.8	97.4
HybridCR [54]	1%	51.9	97.6
SQN [49]	0.1%	50.8	95.5
SLidR [64]	0.08%	53.1	93.2
Tianfang Sun et.al [53]	0.08%	63.7	98.2
Our (Scatter-KITTI)	0.02%	42.8	68.4

Table 4: Quantitative results of different approaches on Nuscenes validation set

Method	Annot.	mIoU(%)	SS/FS(%)
SLidR [64]	0.8%	70.1	94.0
Tianfang Sun et.al [53]	0.8%	77.5	98.4
Our (Scatter-Nuscenes)	0.2%	68.9	75.1

Table 5: Effect of Network components on the SemanticKITTI validation set. **PCL** indicates Perceptual consistency loss

baseline	MM-ScatterNet			mIoU
	2d image	projected point	PCL	
✓				40.6
✓	✓			41.8
✓	✓	✓		42.6
✓	✓	✓	✓	43.8

Table 6: Comparison with different Consistency loss.

Method	mIoU
Hinton et.al [58]	41.2
xMUDA [42]	42.1
PMF [41]	40.2
2DPASS [43]	41.6
Our	43.8

Table 7: Comparing with other multimodal fusion structures.

Method	mIoU
Baseline	40.6
xMUDA [42]	40.7
PMF [41]	39.0
2DPASS [43]	41.0
Our	42.6

knowledge provided by fused features. In addition, we found that projecting point clouds onto a 2D image coordinate system and multi-scale fusion of image features can slightly improve performance by 0.8%. Finally, we found that the perceptual loss function can further extract the fusion features into the point cloud mode, which can achieve about 1.2% performance improvement.

5.2.2 comparing with other Consistency loss.

In order to further verify the effectiveness of our knowledge distillation compared with other methods, as shown in Table 6 where we use other methods to replace the perceptual consistency loss using MM-ScatterNet for fair comparison. We chose the pure knowledge distillation loss function proposed by Hinton, who is a pioneer in this research field. In addition, we also selected the methods proposed by xMUDA [42], PMF [41], and 2DPASS [43] et al., all of which have been proposed in recent years. As shown in Table 6, the application of pure knowledge extraction method[58] in LiDAR semantic segmentation has limited effectiveness in extracting multimodal knowledge. [42] adopts cross-modal feature alignment technique in the task of domain adaptation on semantic segmentation. However, their improvement is still marginal. [41] proposes perceptual loss is bidirectional, so it is not possible to decouple multimodal features from single modal features. Recently, 2DPASS [43] proposed multi-scale fusion to single knowledge utilization (MSFSKD), but this method lacks information perception between modalities, resulting in low confidence fusion information or image information being extracted into point cloud modalities. Finally, our method performs better in Table 6, which shows the effectiveness of our perceptual consistency loss s in extracting multimodal knowledge into point cloud.

5.2.3 Comparing with other multimodal fusion structures.

To further validate the advantages of our fusion scheme, we compared the currently popular multimodal fusion framework with our method. Since xMUDA[42] is a study of cross-modal unsupervised domain adaptation for semantic segmentation, we reconstructed this method. Specifically, we use 2DPASS[43] as the basic framework, remove multi-scale intermediate layers, and use two segmentation heads to handle segmentation and modal fusion, forming the xMUDA[42]. In order to eliminate the influence of distillation loss function, KL divergence is used in all methods. From Table 7, owing to the lack of feature level fusion between point clouds and images, the improvement in baseline model performance is limited. PMF[41] projects the point clouds onto the image plane, which can effectively perform feature fusion. However, this method requires aligning the image and point cloud on the timestamp during testing, making it difficult to apply in practice.

2DPASS [43] is similar to the xMUDA [42]. The difference lies in its fusion of intermediate feature layers, which lifts the middle layer features of the decoding stage 2D image to 3D space for multi-scale fusion with point clouds. Our method is most similar to 2DPASS[43]. The difference is that we not only fuse the image features in the decoding stage, but also fuse the projected 3D point cloud features in the encoding stage of the image, resulting in better performance than the former, as shown in Table 7. In summary, from the above experiments, it can be seen that multi-scale feature fusion can significantly improve the performance of multimodal point cloud segmentation networks.

6 Conclusion

This study proposes a novel weakly supervised learning approach to tackle the expensive and time-consuming dense annotation of point clouds for semantic segmentation. We utilize scatter image annotations and foundation model to generate labels for 3D point clouds. Using the MM-ScatterNet network, which integrates point cloud and image modal features, we achieve high-performance semantic segmentation with limited point label. With the abundance of image data, acquiring large 2D models is relatively easier. Future research can concentrate on enhancing pre-trained foundation models to acquire more accurate 3D pseudo-labels. Further improvement in segmentation performance can be achieved by filtering pseudo-labels through methods like active learning. These advancements aim to maximize data efficiency, reduce annotation workload, and propel advancements in LiDAR segmentation.

References

- [1] Jiaming Liu, Yue Wu, Maoguo Gong, Qiguang Miao, Wenping Ma, and Cai Xu. Exploring dual representations in large-scale point clouds: A simple weakly supervised semantic segmentation framework. In *Proceedings of the 31st ACM International Conference on Multimedia*, pages 2371–2380, 2023.
- [2] Cheng-Kun Yang, Ji-Jia Wu, Kai-Syun Chen, Yung-Yu Chuang, and Yen-Yu Lin. An ml-derived transformer for weakly supervised point cloud segmentation. In *Proceedings of the IEEE/CVF conference on computer vision and pattern recognition*, pages 11830–11839, 2022.
- [3] Baochen Yao, Hui Xiao, Jiayan Zhuang, and Chengbin Peng. Weakly supervised learning for point cloud semantic segmentation with dual teacher. *IEEE Robotics and Automation Letters*, 2023.
- [4] Yongyi Su, Xun Xu, and Kui Jia. Weakly supervised 3d point cloud segmentation via multi-prototype learning. *IEEE Transactions on Circuits and Systems for Video Technology*, 2023.
- [5] Alexander Kirillov, Eric Mintun, Nikhila Ravi, Hanzi Mao, Chloe Rolland, Laura Gustafson, Tete Xiao, Spencer Whitehead, Alexander C Berg, Wan-Yen Lo, et al. Segment anything. In *Proceedings of the IEEE/CVF International Conference on Computer Vision*, pages 4015–4026, 2023.
- [6] Kyle Genova, Xiaoqi Yin, Abhijit Kundu, Caroline Pantofaru, Forrester Cole, Avneesh Sud, Brian Brewington, Brian Shucker, and Thomas Funkhouser. Learning 3d semantic segmentation with only 2d image supervision. In *2021 International Conference on 3D Vision (3DV)*, pages 361–372. IEEE, 2021.
- [7] Haiyan Wang, Xuejian Rong, Liang Yang, Jinglun Feng, Jizhong Xiao, and Yingli Tian. Weakly supervised semantic segmentation in 3d graph-structured point clouds of wild scenes. *arXiv preprint arXiv:2004.12498*, 2020.
- [8] Aloisio Dourado, Frederico Guth, and Teofilo de Campos. Data augmented 3d semantic scene completion with 2d segmentation priors. In *Proceedings of the IEEE/CVF Winter Conference on Applications of Computer Vision*, pages 3781–3790, 2022.
- [9] Ziyi Wang, Yongming Rao, Xumin Yu, Jie Zhou, and Jiwen Lu. Semaffinet: Semantic-affine transformation for point cloud segmentation. In *Proceedings of the IEEE/CVF Conference on Computer Vision and Pattern Recognition*, pages 11819–11829, 2022.
- [10] Jens Behley, Martin Garbade, Andres Milioto, Jan Quenzel, Sven Behnke, Cyrill Stachniss, and Jurgen Gall. Semantickitti: A dataset for semantic scene understanding of lidar sequences. In *Proceedings of the IEEE/CVF international conference on computer vision*, pages 9297–9307, 2019.
- [11] Holger Caesar, Varun Bankiti, Alex H Lang, Sourabh Vora, Venice Erin Liong, Qiang Xu, Anush Krishnan, Yu Pan, Giancarlo Baldan, and Oscar Beijbom. nuscenes: A multimodal dataset for autonomous driving. In *Proceedings of the IEEE/CVF conference on computer vision and pattern recognition*, pages 11621–11631, 2020.
- [12] Charles R Qi, Hao Su, Kaichun Mo, and Leonidas J Guibas. Pointnet: Deep learning on point sets for 3d classification and segmentation. In *Proceedings of the IEEE conference on computer vision and pattern recognition*, pages 652–660, 2017.
- [13] Lin-Zhuo Chen, Xuan-Yi Li, Deng-Ping Fan, Kai Wang, Shao-Ping Lu, and Ming-Ming Cheng. Lsanet: Feature learning on point sets by local spatial aware layer. *arXiv preprint arXiv:1905.05442*, 2019.
- [14] Kang Zhiheng and Li Ning. Pyramnet: Point cloud pyramid attention network and graph embedding module for classification and segmentation. *arXiv preprint arXiv:1906.03299*, 2019.
- [15] Yangyan Li, Rui Bu, Mingchao Sun, Wei Wu, Xinhan Di, and Baoquan Chen. Pointcnn: Convolution on x-transformed points. *Advances in neural information processing systems*, 31, 2018.
- [16] Artem Komarichev, Zichun Zhong, and Jing Hua. A-cnn: Annularly convolutional neural networks on point clouds. In *Proceedings of the IEEE/CVF conference on computer vision and pattern recognition*, pages 7421–7430, 2019.
- [17] Hugues Thomas, Charles R Qi, Jean-Emmanuel Deschaud, Beatriz Marcotegui, François Goulette, and Leonidas J Guibas. Kpconv: Flexible and deformable convolution for point clouds. In *Proceedings of the IEEE/CVF international conference on computer vision*, pages 6411–6420, 2019.
- [18] W Wu, Z Qi, and F PointConv Li. Deep convolutional networks on 3d point clouds. *IEEE In CVF Conference on Computer Vision and Pattern Recognition (CVPR)*, pages 9613–9622, 2019.
- [19] Mutian Xu, Runyu Ding, Hengshuang Zhao, and Xiaojuan Qi. Paconv: Position adaptive convolution with dynamic kernel assembling on point clouds. In *Proceedings of the IEEE/CVF Conference on Computer Vision and Pattern Recognition*, pages 3173–3182, 2021.

- [20] Francis Engelmann, Theodora Kontogianni, Alexander Hermans, and Bastian Leibe. Exploring spatial context for 3d semantic segmentation of point clouds. In *Proceedings of the IEEE international conference on computer vision workshops*, pages 716–724, 2017.
- [21] Ruoyu Li, Sheng Wang, Feiyun Zhu, and Junzhou Huang. Adaptive graph convolutional neural networks. In *Proceedings of the AAAI conference on artificial intelligence*, volume 32, 2018.
- [22] Yue Wang, Yongbin Sun, Ziwei Liu, Sanjay E Sarma, Michael M Bronstein, and Justin M Solomon. Dynamic graph cnn for learning on point clouds. *Acm Transactions On Graphics (tog)*, 38(5):1–12, 2019.
- [23] Jonathan Long, Evan Shelhamer, and Trevor Darrell. Fully convolutional networks for semantic segmentation. In *Proceedings of the IEEE conference on computer vision and pattern recognition*, pages 3431–3440, 2015.
- [24] Olaf Ronneberger, Philipp Fischer, and Thomas Brox. U-net: Convolutional networks for biomedical image segmentation. In *Medical Image Computing and Computer-Assisted Intervention–MICCAI 2015: 18th International Conference, Munich, Germany, October 5-9, 2015, Proceedings, Part III 18*, pages 234–241. Springer, 2015.
- [25] Felix Järemo Lawin, Martin Danelljan, Patrik Tosteberg, Goutam Bhat, Fahad Shahbaz Khan, and Michael Felsberg. Deep projective 3d semantic segmentation. In *Computer Analysis of Images and Patterns: 17th International Conference, CAIP 2017, Ystad, Sweden, August 22-24, 2017, Proceedings, Part I 17*, pages 95–107. Springer, 2017.
- [26] Alexandre Boulch, Bertrand Le Saux, Nicolas Audebert, et al. Unstructured point cloud semantic labeling using deep segmentation networks. *3dor@ eurographics*, 3:17–24, 2017.
- [27] Ziyu Zhao, Zhenyao Wu, Xinyi Wu, Canyu Zhang, and Song Wang. Crossmodal few-shot 3d point cloud semantic segmentation. In *Proceedings of the 30th ACM International Conference on Multimedia*, pages 4760–4768, 2022.
- [28] Eren Erdal Aksoy, Saimir Baci, and Selcuk Cavdar. Salsanet: Fast road and vehicle segmentation in lidar point clouds for autonomous driving. In *2020 IEEE intelligent vehicles symposium (IV)*, pages 926–932. IEEE, 2020.
- [29] Inigo Alonso, Luis Riazuelo, Luis Montesano, and Ana C Murillo. 3d-mininet: Learning a 2d representation from point clouds for fast and efficient 3d lidar semantic segmentation. *IEEE Robotics and Automation Letters*, 5(4):5432–5439, 2020.
- [30] Tiago Cortinhal, George Tzelepis, and Eren Erdal Aksoy. Salsanext: Fast, uncertainty-aware semantic segmentation of lidar point clouds. In *Advances in Visual Computing: 15th International Symposium, ISVC 2020, San Diego, CA, USA, October 5–7, 2020, Proceedings, Part II 15*, pages 207–222. Springer, 2020.
- [31] Bichen Wu, Xuanyu Zhou, Sicheng Zhao, Xiangyu Yue, and Kurt Keutzer. Squeezesegv2: Improved model structure and unsupervised domain adaptation for road-object segmentation from a lidar point cloud. In *2019 International Conference on Robotics and Automation (ICRA)*, pages 4376–4382. IEEE, 2019.
- [32] Martin Gerdzhev, Ryan Razani, Ehsan Taghavi, and Liu Bingbing. Tornado-net: multiview total variation semantic segmentation with diamond inception module. In *2021 IEEE International Conference on Robotics and Automation (ICRA)*, pages 9543–9549. IEEE, 2021.
- [33] Venice Erin Liong, Thi Ngoc Tho Nguyen, Sergi Widjaja, Dhananjai Sharma, and Zhuang Jie Chong. Amvnet: Assertion-based multi-view fusion network for lidar semantic segmentation. *arXiv preprint arXiv:2012.04934*, 2020.
- [34] Benjamin Graham, Martin Engelcke, and Laurens Van Der Maaten. 3d semantic segmentation with submanifold sparse convolutional networks. In *Proceedings of the IEEE conference on computer vision and pattern recognition*, pages 9224–9232, 2018.
- [35] Hui Zhou, Xinge Zhu, Xiao Song, Yuexin Ma, Zhe Wang, Hongsheng Li, and Dahua Lin. Cylinder3d: An effective 3d framework for driving-scene lidar semantic segmentation. *arXiv preprint arXiv:2008.01550*, 2020.
- [36] Ran Cheng, Ryan Razani, Ehsan Taghavi, Enxu Li, and Bingbing Liu. 2-s3net: Attentive feature fusion with adaptive feature selection for sparse semantic segmentation network. In *Proceedings of the IEEE/CVF conference on computer vision and pattern recognition*, pages 12547–12556, 2021.
- [37] Haotian Tang, Zhijian Liu, Shengyu Zhao, Yujun Lin, Ji Lin, Hanrui Wang, and Song Han. Searching efficient 3d architectures with sparse point-voxel convolution. In *Computer Vision–ECCV 2020: 16th European Conference, Glasgow, UK, August 23–28, 2020, Proceedings, Part XXVIII*, pages 685–702. Springer, 2020.
- [38] Jianyun Xu, Ruixiang Zhang, Jian Dou, Yushi Zhu, Jie Sun, and Shiliang Pu. Rpvnet: A deep and efficient range-point-voxel fusion network for lidar point cloud segmentation. In *Proceedings of the IEEE/CVF International Conference on Computer Vision*, pages 16024–16033, 2021.

- [39] Ming Liang, Bin Yang, Yun Chen, Rui Hu, and Raquel Urtasun. Multi-task multi-sensor fusion for 3d object detection. In *Proceedings of the IEEE/CVF Conference on Computer Vision and Pattern Recognition*, pages 7345–7353, 2019.
- [40] Ming Liang, Bin Yang, Shenlong Wang, and Raquel Urtasun. Deep continuous fusion for multi-sensor 3d object detection. In *Proceedings of the European conference on computer vision (ECCV)*, pages 641–656, 2018.
- [41] Zhuangwei Zhuang, Rong Li, Kui Jia, Qicheng Wang, Yuanqing Li, and Mingkui Tan. Perception-aware multi-sensor fusion for 3d lidar semantic segmentation. In *Proceedings of the IEEE/CVF International Conference on Computer Vision*, pages 16280–16290, 2021.
- [42] Maximilian Jaritz, Tuan-Hung Vu, Raoul de Charette, Emilie Wirbel, and Patrick Pérez. xmuda: Cross-modal unsupervised domain adaptation for 3d semantic segmentation. In *Proceedings of the IEEE/CVF conference on computer vision and pattern recognition*, pages 12605–12614, 2020.
- [43] Xu Yan, Jiantao Gao, Chaoda Zheng, Chao Zheng, Ruimao Zhang, Shuguang Cui, and Zhen Li. 2dpass: 2d priors assisted semantic segmentation on lidar point clouds. In *Computer Vision—ECCV 2022: 17th European Conference, Tel Aviv, Israel, October 23–27, 2022, Proceedings, Part XXVIII*, pages 677–695. Springer, 2022.
- [44] Jingyi Wang, Yu Liu, Hanlin Tan, and Maojun Zhang. A survey on weakly supervised 3d point cloud semantic segmentation. *IET Computer Vision*, 2023.
- [45] Zhengzhe Liu, Xiaojuan Qi, and Chi-Wing Fu. One thing one click: A self-training approach for weakly supervised 3d semantic segmentation. In *Proceedings of the IEEE/CVF Conference on Computer Vision and Pattern Recognition*, pages 1726–1736, 2021.
- [46] Yachao Zhang, Zonghao Li, Yuan Xie, Yanyun Qu, Cuihua Li, and Tao Mei. Weakly supervised semantic segmentation for large-scale point cloud. In *Proceedings of the AAAI Conference on Artificial Intelligence*, volume 35, pages 3421–3429, 2021.
- [47] Jiacheng Wei, Guosheng Lin, Kim-Hui Yap, Tzu-Yi Hung, and Lihua Xie. Multi-path region mining for weakly supervised 3d semantic segmentation on point clouds. In *Proceedings of the IEEE/CVF conference on computer vision and pattern recognition*, pages 4384–4393, 2020.
- [48] Xiawei Li, Qingyuan Xu, Jing Zhang, Tianyi Zhang, Qian Yu, Lu Sheng, and Dong Xu. Multi-modality affinity inference for weakly supervised 3d semantic segmentation. In *Proceedings of the AAAI Conference on Artificial Intelligence*, volume 38, pages 3216–3224, 2024.
- [49] Qingyong Hu, Bo Yang, Guangchi Fang, Yulan Guo, Aleš Leonardis, Niki Trigoni, and Andrew Markham. Sqn: Weakly-supervised semantic segmentation of large-scale 3d point clouds. In *European Conference on Computer Vision*, pages 600–619. Springer, 2022.
- [50] Minghua Liu, Yin Zhou, Charles R Qi, Boqing Gong, Hao Su, and Dragomir Anguelov. Less: Label-efficient semantic segmentation for lidar point clouds. In *European conference on computer vision*, pages 70–89. Springer, 2022.
- [51] Bolei Zhou, Aditya Khosla, Agata Lapedriza, Aude Oliva, and Antonio Torralba. Learning deep features for discriminative localization. In *Proceedings of the IEEE conference on computer vision and pattern recognition*, pages 2921–2929, 2016.
- [52] Zhonghua Wu, Yicheng Wu, Guosheng Lin, Jianfei Cai, and Chen Qian. Dual adaptive transformations for weakly supervised point cloud segmentation. In *European conference on computer vision*, pages 78–96. Springer, 2022.
- [53] Tianfang Sun, Zhizhong Zhang, Xin Tan, Yanyun Qu, and Yuan Xie. Image understands point cloud: Weakly supervised 3d semantic segmentation via association learning. *IEEE Transactions on Image Processing*, 2024.
- [54] Mengtian Li, Yuan Xie, Yunhang Shen, Bo Ke, Ruizhi Qiao, Bo Ren, Shaohui Lin, and Lizhuang Ma. Hybridcr: Weakly-supervised 3d point cloud semantic segmentation via hybrid contrastive regularization. In *Proceedings of the IEEE/CVF conference on computer vision and pattern recognition*, pages 14930–14939, 2022.
- [55] Andreas Geiger, Philip Lenz, Christoph Stiller, and Raquel Urtasun. Vision meets robotics: The kitti dataset. *The International Journal of Robotics Research*, 32(11):1231–1237, 2013.
- [56] Kaiming He, Xiangyu Zhang, Shaoqing Ren, and Jian Sun. Deep residual learning for image recognition. In *Proceedings of the IEEE conference on computer vision and pattern recognition*, pages 770–778, 2016.
- [57] Alfréd Rényi. On measures of entropy and information. In *Proceedings of the Fourth Berkeley Symposium on Mathematical Statistics and Probability, Volume 1: Contributions to the Theory of Statistics*, volume 4, pages 547–562. University of California Press, 1961.
- [58] Geoffrey Hinton, Oriol Vinyals, and Jeff Dean. Distilling the knowledge in a neural network. *arXiv preprint arXiv:1503.02531*, 2015.

- [59] Maxim Berman, Amal Rannen Triki, and Matthew B Blaschko. The lovász-softmax loss: A tractable surrogate for the optimization of the intersection-over-union measure in neural networks. In *Proceedings of the IEEE conference on computer vision and pattern recognition*, pages 4413–4421, 2018.
- [60] Christopher Choy, JunYoung Gwak, and Silvio Savarese. 4d spatio-temporal convnets: Minkowski convolutional neural networks. In *Proceedings of the IEEE/CVF conference on computer vision and pattern recognition*, pages 3075–3084, 2019.
- [61] Xin Lai, Yukang Chen, Fanbin Lu, Jianhui Liu, and Jiaya Jia. Spherical transformer for lidar-based 3d recognition. In *Proceedings of the IEEE/CVF Conference on Computer Vision and Pattern Recognition*, pages 17545–17555, 2023.
- [62] Ozan Unal, Dengxin Dai, and Luc Van Gool. Scribble-supervised lidar semantic segmentation. In *Proceedings of the IEEE/CVF Conference on Computer Vision and Pattern Recognition*, pages 2697–2707, 2022.
- [63] Tsung-Han Wu, Yueh-Cheng Liu, Yu-Kai Huang, Hsin-Ying Lee, Hung-Ting Su, Ping-Chia Huang, and Winston H Hsu. Redal: Region-based and diversity-aware active learning for point cloud semantic segmentation. In *Proceedings of the IEEE/CVF international conference on computer vision*, pages 15510–15519, 2021.
- [64] Corentin Sautier, Gilles Puy, Spyros Gidaris, Alexandre Boulch, Andrei Bursuc, and Renaud Marlet. Image-to-lidar self-supervised distillation for autonomous driving data. In *Proceedings of the IEEE/CVF Conference on Computer Vision and Pattern Recognition*, pages 9891–9901, 2022.